1998

Attitude Measurement

Mark A. Stedham
University of Alabama, Huntsville

Partha P. Banerjee
University of Dayton, pbanerjee1@udayton.edu

Seiji Nishifuji
Yamaguchi University

Shogo Tanaka
Yamaguchi University

10.2 Attitude Measurement

Mark A. Stedham, Partha P. Banerjee, Seiji Nishfuji, and Shogo Tanaka

In many practical situations, it is important to determine and measure the attitude of a particular vehicle, such as a ship, an airplane, a piece of mechanical equipment such as a crane lifter, or a spacecraft. For this reason, many attitude sensors have been developed with advanced computer and semiconductor technologies. This section first introduces the various attitude sensors with an explanation of their operating principles and then presents several methodologies for attitude measurement and determination, including ships and crane lifters, aircraft, and spacecraft applications.

Attitude Sensors for Ships, Aircraft, and Crane Lifters

There are many types of gyroscopes that, corresponding to the physical measurement mechanisms used, may be classified as two-axes *freedom gyro* and single-axis freedom gyro using precession, *vibratory gyro* using Coriolis' force, and *optic gyro* using Sagnac's effect. Among them, the two-axes freedom gyro has the longest history. It consists of a high-speed rotating rotor around a spin axis supported by two orthogonal axes. This type of gyro is generally classified as either a *free gyro*, a *vertical gyro* (VG), or a *directional gyro* (DG).

The single-axis freedom gyro has only one output axis in addition to the spin axis. Depending on the specifications (in which) the gyro is designed, there are two types of gyros, the *rate gyro and* the *rate integrating gyro.* Related to these rotating-type gyros is another type of gyro known as the *electrostatic gyro*, which makes use of a high-speed rotating sphere in a vacuum cavity. Because of its resistance-free property, the electrostatic gyro has the highest accuracy among existing gyros. There are also rotorless gyros. The first one is a vibratory gyro that uses Coriolis' force as the measurement principle. The second type is an optical one. Among optical gyros, there are two types: the *ring laser gyro* and the *fiber optic gyro.* Both rely on the Sagnac effect in their measurement mechanisms. The performance of gyros is evaluated by their drift rates, and the performance of various gyros is shown in Table 10.2, for reference, with their primary usages.

Recently, with the development of computer technology, many types of three-axes gyros have been developed that can measure not only the tilt angles but also the angular velocities and the accelerations along the three axes by combining several gyros and accelerometers. Accelerometers are often coupled with gyros to provide flight and ship navigation systems as well as attitude sensors for dynamic objects such as crane lifters. Examples include the *attitude and heading reference system* (AHRS), *inertial navigation system* (INS), *inertial measurement unit* (IMU), and *gyro compass* (GC), as well as the VGs and DGs discussed above [1].

TABLE 10.2 Performance of Different Types of Gyros

Type of the gyro	Degrees of freedom	Quantities to be detected	Accuracy (° h^{-1})
Free gyro	2	Angle	1
Vertical gyro	2	Declination from horizontal plane	1
Directional gyro	2	Shift from reference direction	1
Rate gyro	1	Angular velocity	10
Rate integrating gyro	1	Angle	0.001–1
Ring laser gyro	1	Angular velocity	0.003
Fiber optic gyro	1	Angular velocity	0.01
Electrostatic gyro	2	Angle	0.00001–0.01

The principle of a servo-type accelerometer is explained below (see Figure 10.8). As soon as the shift of the beam caused by the acceleration α is detected by the deflection pickup, the current i is generated by the servo-amplifier, which produces a torque to keep the beam at the principle axis of the sensor. Since the torque and the current that generates the torque are proportional to α, the acceleration can be measured using the current. The measurement process forms a closed-loop system, so that the sensor is not only robust to disturbances, but also achieves a high measurement accuracy (see Table 10.3).

Similarly, an inclinometer is another inertial sensor that measures tilt angle to provide attitude information (see Figure 10.9). The principle of servo-type inclinometers is the same as that of the servo-type accelerometer, except that the beam in the accelerometer is replaced by a pendulum suspended from the supporting point in the sensor. When the sensor is placed on the inclined static surface of tilt angle β, the pendulum takes the angle β against the principle axis of the sensor, assuming the sensor has no force other than gravity acting on it. The sensor can, however, generate a torque $T_c = mgl\sin\beta \cong mgl\beta$ to keep the pendulum at the principle axis, then the tilt angle β can be accurately measured using the torque (and consequently the current producing the torque), where m and l are the pendulum mass and length of the pendulum to its mass center, respectively. One must note, however, that such a sensor is essentially designed to measure the tilt angles of static inclined surfaces. Thus, when applied to dynamic inclined surfaces, the accelerations will affect the torque, making the sensor unreliable. An intelligent attitude

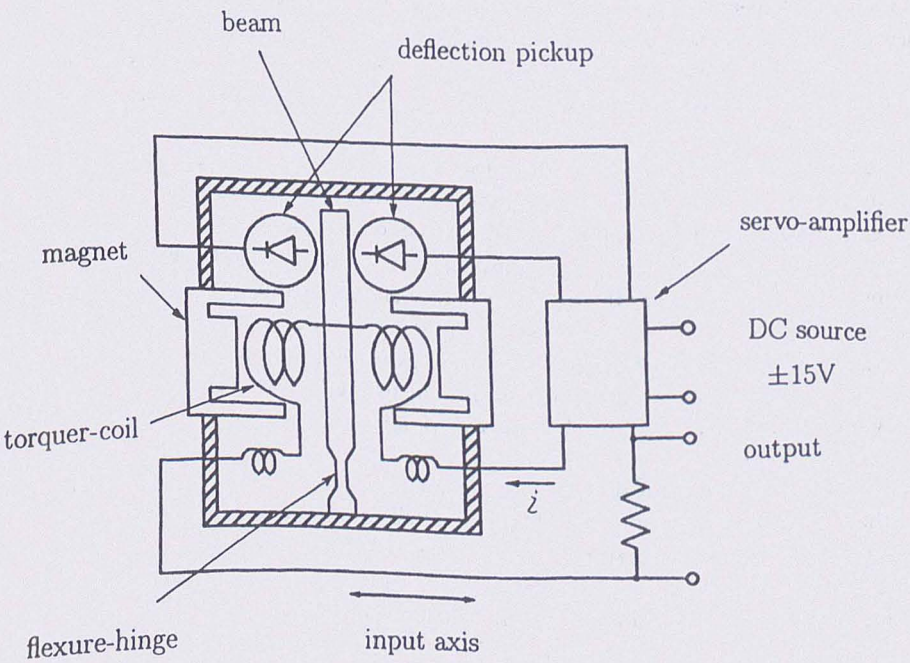

FIGURE 10.8 Servo-type accelerometer.

TABLE 10.3 Specification of a Servo-Type Accelerometer

Measurement range	±5 *g*
Resolution	Less than 5 μ*g* (dc)
Sensitivity	2 V g^{-1}
Output resistance	560 Ω
Torquer current	3.5 mA g^{-1}
Case alignment	Less than ±1°
Frequency response	450 Hz (±3 dB)
Temperature range	−25 to +70°C
Power source	±15 V (dc)
Consumption current	Less than 15 mA
Size	28.4 mm × 24.5 mm
Mass	46 *g* (including the cable 10 *g*)

Note: g: gravitational acceleration (according to the type TA-25D-05 by TOKIMEC).

sensing system that overcomes such difficulty will be introduced later. Although application is limited to static inclined surfaces with minute tilt angles, a dielectric-type inclinometer employing electrodes and a bubble kept in an electrolyte can achieve high accuracies on the order of 10^{-4}°.

Attitude Sensors for Spacecraft Applications

Attitude measurement for spacecraft usually requires two or more sensors for detecting the reference sources needed to satisfy attitude requirements. The choice of which sensors to employ is primarily influenced by the direction the spacecraft is usually pointing as well as the accuracy requirements for attitude determination [2]. Table 10.4 summarizes some performance parameters for these sensors as well as typical manufacturers.

Inertial measurement units generally consist of gyroscopes coupled with accelerometers, which together measure both rotational and translational motion. These IMUs may be either gimbal mounted (movement about a gimbal point, independent of the spacecraft) or a strapdown system (rigidly mounted to the spacecraft body), where expansive software is used to convert sensor outputs into reference frame measurements. IMUs tend to suffer gyro drift and other bias errors and, when used for spacecraft attitude measurements, are often used with one or more of the sensors discussed below.

Sun sensors detect the visible light from the sun, measuring the angle between the sun's radiation and the detector's photocell. The sun is a commonly chosen attitude reference source since it is by far the

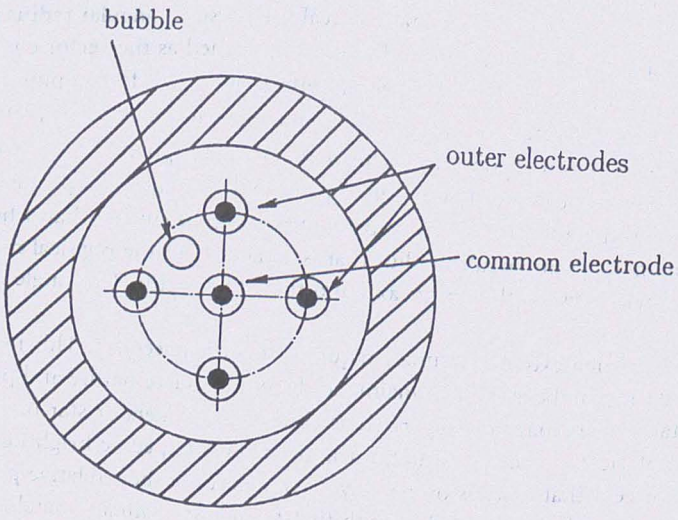

FIGURE 10.9 Dielectric-type inclinometer (front view).

TABLE 10.4 Spacecraft Attitude Determination Sensors

Sensor	Accuracy	Mass (kg)	Typical vendors
IMU	1 to 5 × 10^{-6} *g*	3 to 25	Northrop Grumman, Bendix, Kearfott,Honeywell, Hamilton, Standard, Litton, Teledyne
Sun Sensor	10^{-2} to 3°	0.5 to 2	Adcole, TRW, Ball Aerospace
Horizon Sensor	10^{-1} to 1°	2 to 5	Barnes, Ithaco, Lockheed Martin, Lockheed Barnes
Star Sensor	10^{-3} to 10^{-2}°	3 to 7	Ball Aerospace, Bendix, Honeywell, Hughes
Magnetometer	0.5 to 3°	~1	Schonstedt, Develco

Adapted from Larsen, W. J. and Wertz, J. R., Eds., *Space Mission Analysis and Design*, Torrance, CA: Microcosm Inc. and Dordrecht, The Netherlands: Kluwer Academic Publishers, 1992, p.360.

visually brightest object in the sky, having a total radiation per unit area of 1353 W m^{-2} at Earth distances [3]. Also, it is generally accepted as a valid point source for most attitude applications, having an angular radius of 0.25° at Earth distances. Increased measurement accuracy can be obtained by determining its centroid. Even though sun sensors are quite accurate (0.01° to 3.0°), they do require clear fields of view, and sometimes suffer periods of eclipse from both the Earth and the moon [4]. Also, sensitive equipment (such as imaging devices) must be protected from the powerful radiation of direct sunlight. When the sun is available, the angle between it and the sensor's primary axis is referred to as the *sun angle.*

For spacecraft in near-Earth orbits, the Earth is the second brightest object in the sky and covers as much as 40% of the sky. Earth *horizon sensors* detect the interface between the Earth's edge (or limb) and the space background. Horizon sensors can detect either of the Earth's visible limb (albedo sensor), infrared limb, or air glow. The infrared limb is the edge between the warm Earth and the cold space background. The air glow is a region of the atmosphere around the Earth that is visible to the spacecraft when it is on the night side of the Earth. Accuracies for horizon sensors are in the 0.1° to 1.0° range. Increased accuracy requires Earth oblate spheroid modeling [4]. Some problems associated with albedo detection include the distortion effects of the Earth's atmosphere, falsely identifying the day/night terminator crossing as the true Earth limb, and the considerable variability of the Earth's albedo in the visible spectrum (varies from land, sea, ice).

Most sensors used to detect the Earth's horizon are scanning sensors with narrow fields of view that measure the time between horizon crossings. In general, two horizon crossings occur per sensor scan period: one crossing when the sensor scans from the space background onto the Earth, followed by a second crossing when the sensor scans from the Earth back to space. The combination of horizon crossing times, scan rate, and spacecraft altitude allows for the computation of the Earth's apparent *angular radius.* The apparent angular radius will be smaller than the real (or physical) angular radius if the spacecraft is tilted away from the Earth nadir vector. The nadir vector is defined as the vector connecting the center of the spacecraft to the center of the Earth. To see this effect, one needs to compute the Earth's physical radius ρ, which for a given spacecraft altitude h (in kilometers), is given by $\rho = \sin^{-1}[(6371)/(6371 + h)]$.

If the spacecraft horizon sensor is pointing exactly *nadir,* then the apparent angular radius as measured by the sensor will agree with the physical radius given by the above relation for ρ. However, if the horizon sensor is pointed away from nadir, the horizon crossing times will be smaller than when pointing exactly nadir. This results in an apparent angular radius that is smaller than the physical radius by an amount proportional to the angle between the sensor axis and the nadir vector. This angle is referred to as the *nadir angle.*

Star sensors are used when extreme accuracy requirements are necessary. This high degree of sensor accuracy (0.003° to 0.01°) can be attributed mainly to the point source nature and precise fixed location of stars in space. Star sensors may be categorized as either star trackers or star mappers. A star tracker utilizes a wide field of view in order to search for a given star of specific brightness. A star mapper is similar to a tracker, except that it scans over many stars, recording their relative positions and angular separations. By comparing the recorded data with that from a *star catalog* (database), exact spacecraft

orientation can be obtained. The angle between the star line-of-sight and the sensor's primary axis is referred to as the *star angle.*

The accuracy of star sensors is obtained with higher costs, however. Star sensors are generally heavier and consume more power than other types of attitude sensors. In addition, star sensors are quite sensitive to stray light sources such as sunlight reflected from the spacecraft or the Earth and sunlight scattered from dust particles and jet exhausts [4]. Most rely on optical shielding to reduce the effects of stray light.

Magnetic sensors (called *magnetometers*) measure both the magnitude and direction of the Earth's magnetic field. The difference in orientation between the measured field and the true field translates into attitude determination. Magnetometer accuracies (0.5° to 3.0°) are usually less than the other sensor types because of the uncertainty in the Earth's true field, which tends to change or shift over time. In addition, the Earth's magnetic field decreases with increasing altitude, and magnetometers are generally limited to altitudes of about 6000 km. For this reason, magnetometers are often used with one of the other sensor types already discussed for improved measurement accuracy [2].

Automatic On-Line Attitude Measurement for Ships and Crane Lifters

For on-line attitude measurement for ships and crane lifters, the first thing that comes to mind is to use gyros. However, because they often suffer from drifts, accurate attitude measurements might not be achieved using the gyros. Accordingly, one uses attitude on-line measurement systems that do not utilize gyros but servo-type accelerometers and inclinometers. The philosophy of the measurement systems introduced here is to make the best use of the system dynamics of the object and the sensors and to apply Kalman filters or adaptive filters to achieve high measurement accuracy.

Attitude Measurement for Ships

On-line accurate measurement of a ship's attitude is extremely important in exact search of the seabed patterns with sonars [5, 6]. It is also required by high-performance ships like hovercrafts from the viewpoint of suppressing swings by the waves. The measurement of a ship's attitude can usually be reduced to that of the heaving, rolling, and pitching of the ship. For such a measurement, a heave sensor has been used, whose output is given by double integration of the output of an accelerometer vertically directed with a gyroscope. However, since the initial values of heaving displacement and its velocity are unknown, the output will contain a bias that increases with time, and the accuracy of the sensor deteriorates considerably. From this viewpoint, one introduces a strapdown-type on-line measurement system that adequately processes the outputs of the two servo-type inclinometers and one accelerometer mounted on the ship [7].

Location of Sensors and Outputs

The two servo-type inclinometers and one servo-type accelerometer are located on the deck (at the point A) of vertical distance L from O, the intersection of rolling and pitching axes (see Figure 10.10).The two inclinometers are set in such a way that the rolling and the pitching angles are measured respectively. The accelerometer is set upward to the deck to obtain the information on the heaving. Because inclinometers were originally developed for the measurement of the tilt angles of static inclined surfaces, the rigid pendulum inside the sensor is considerably affected by the ship's acceleration other than the gravitational one. Applying Lagrange's equations of motion [8, 9] to rigid pendulums and calculating the torques to keep their deflections from the principal axes almost zero yields the sensor outputs [7]:

$$z_1(t) = \theta(t) - \frac{L}{g}\ddot{\theta}(t) + v_1(t) \tag{10.45}$$

$$z_2(t) = p(t) - \frac{L}{g}\ddot{p}(t) + v_2(t) \tag{10.46}$$

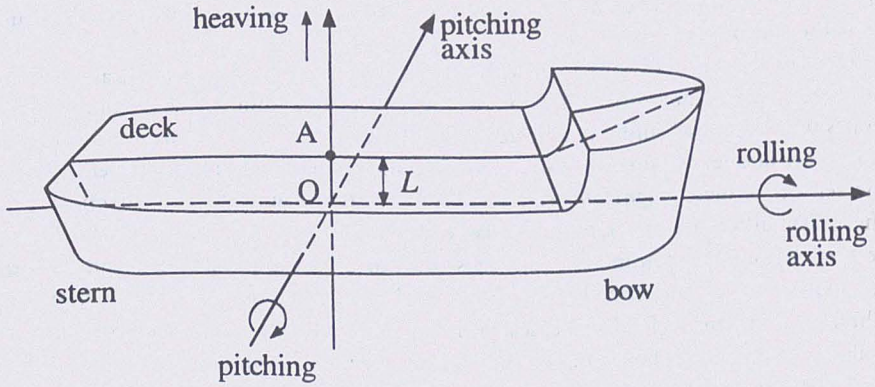

FIGURE 10.10 Location of sensors.

where $z_1(t)$, $z_2(t)$, $\theta(t)$, $p(t)$, and g denote, respectively, the outputs of the two inclinometers, the rolling and the pitching angles, and the gravitational acceleration ($v_1(t)$ and $v_2(t)$: noises of the outputs, including the approximation errors in deriving the outputs).

On the other hand, the accelerometer output is expressed as:

$$z_3(t) = \left(g + \alpha(t)\right)\cos\theta(t)\cos p(t) + v_3(t) \tag{10.47}$$

where $\alpha(t)$ and $v_3(t)$ represent, respectively, the heaving acceleration and the accelerometer noise.

Dynamics of Attitude Signals

It is well known that each of the heaving, rolling, and pitching in inshore seas has two dominant waves in a short interval. That is, a sinusoidal wave of long periodic length (in the range of 6 s to 10 s) and a sinusoidal wave of short periodic length (in the range of 2 s to 3 s) [10–12]. Thus, one model each of the signals in a short interval by a composite wave of the two dominant sinusoidal waves. For the heaving (in a short interval), the displacement is modeled by:

$$x(t) = a_1 \sin\left(\omega_1 t + \varphi_1\right) + a_2 \sin\left(\omega_2 t + \varphi_2\right) \tag{10.48}$$

with the parameters $\{a_i\}$, $\{\varphi_i\}$, and $\{\omega_i\}$ unknown. From the 4th-order differential equation satisfied by the $x(t)$, we obtain the linear dynamic equation [7]:

$$\dot{\mathbf{x}}(t) = A\mathbf{x}(t), \qquad A \equiv \begin{bmatrix} 0 & 1 & 0 & 0 \\ 0 & 0 & 1 & 0 \\ 0 & 0 & 0 & 1 \\ -\omega_1^2\omega_2^2 & 0 & -\left(\omega_1^2 + \omega_2^2\right) & 0 \end{bmatrix} \tag{10.49}$$

where $\mathbf{x}(t) \equiv (x_1, x_2, x_3, x_4)^T$ ($x_n = d^{n-1}x/dt^{n-1}$ ($n = 1, \ldots, 4$)). On the other hand, the rolling and pitching angles can be modeled by:

$$x(t) = a_1 \sin\left(\omega_1 t + \varphi_1\right) + a_2 \sin\left(\omega_2 t + \varphi_2\right) + b \tag{10.50}$$

because there are usually some biases associated with them. From the 5th-order differential equation which Equation 10.50 satisfies, we get the similar state variable representation of the model as

Equation 10.49. In practice, the heaving, rolling, and pitching signals have many nondominant sinusoidal waves in addition to the dominant ones. Therefore, Equation 10.49 is modified by introducing a white Gaussian noise $w(t)$ with zero mean and adequate variance σ^2 as follows:

$$\dot{\mathbf{x}}(t) = A\mathbf{x}(t) + \Gamma w(t) \tag{10.51}$$

where $\Gamma = (0,1,0,0)^T$ for the heaving and $\Gamma = (0,1,0,0,0)^T$ for the rolling and pitching. The higher the order of the models, the better the measurement accuracy will be. If we consider the on-line measurement of the signals, Equation 10.51 will be sufficient.

On-Line Attitude Measurement

The observation Equations 10.45 and 10.46 are expressed using their own state vector $\mathbf{x}(t)$. The observation equations in a discretized form are:

$$y_k = H\mathbf{x}_k + v_k \tag{10.52}$$

where $H = [1,0,-L/g,0,0]$ and y_k, $\mathbf{x}_k$, and v_k, respectively, denote $y(t)$, $\mathbf{x}(t)$, and $v(t)$ of the corresponding signals at the k-th sampling instant [7, 9]. The discretized form of the dynamic Equation 10.51 is:

$$\mathbf{x}_{k+1} = F\mathbf{x}_k + \mathbf{w}_k \tag{10.53}$$

where

$$F \equiv \Phi(t)\Big|_{t=\Delta T}, \quad \Phi(t) \equiv L^{-1}\left\{(sI - A)^{-1}\right\}. \tag{10.54}$$

Here, L^{-1} and ΔT, respectively, denote the inverse Laplace transformation and the sampling period. The discretized transition noise $\mathbf{w}_k$ becomes a white Gaussian noise with zero mean and covariance:

$$W = \sigma^2 \int_0^{\Delta T} \Phi(\Delta T - \tau)\Gamma\Gamma^T\Phi^T(\Delta T - \tau)d\tau \tag{10.55}$$

The measurement of the rolling and pitching can thus be reduced to the state estimation of the linear discrete dynamic systems (Equations 10.52 and 10.53), if the angular frequencies ω_1 and ω_2 are given and v_k is assumed to have a white Gaussian property. The state estimation is achieved by a Kalman filter [7, 13]. However, difficulties in implementing the filter are that the exact values of the two angular frequencies are a priori unknown and also time variant. To overcome the difficulty, adequate candidates $\{(\omega_1^i, \omega_2^i);\ 1 \le i \le M\}$ for the parameters $\{\omega_1, \omega_2\}$ are set and a bank of Kalman filters is used. Then, the final estimate is obtained as the conditional expectation of the state estimate as follows:

$$\hat{\mathbf{x}}^0_{k/k} \equiv \sum_{i=1}^{M} p_k^i \hat{\mathbf{x}}^i_{k/k} \tag{10.56}$$

where $\hat{\mathbf{x}}^i_{k/k}$ represents the state estimate $\hat{\mathbf{x}}_{k/k}$ for the i-th candidate $\Omega_i = (\omega_1^i, \omega_2^i)$, and p_k^i denotes the conditional posteriori probability of the i-th candidate calculated based on the Bayesian theorem:

$$p_k^i = \frac{p\left(y_k / \Omega_i, Y^{k-1}\right) p_{k-1}^i}{\sum_{j=1}^{M} p_{k-1}^j p\left(y_k / \Omega_j, Y^{k-1}\right)} \tag{10.57}$$

Here, $p(y_k/\Omega_i, Y^{k-1})$ represents the conditional Gaussian probability density function of y_k under Ω_i and $Y^{k-1} \equiv \{y_j;\ j \le k-1\}$, whose mean and variance are calculated recursively [7].

The proposed measurement system can adaptively and automatically select the most appropriate candidate versus time. It thus enables an accurate on-line measurement of the rolling and pitching whose dominant angular frequencies vary with time. The first, second, and third components of the final estimate $\hat{\mathbf{x}}^{o}_{k/k}$ represent, respectively, the estimates of the displacement, velocity, and acceleration. The proposed system thus has an advantage in that it can measure not only the displacements, but also the velocities and the accelerations of the three signals. In order to improve the measurement accuracy of the rolling and pitching, one should place the inclinometers near the intersection O of the rolling and the pitching axes.

Finally, the dynamics of the heaving is given by Equation 10.51 similar to that of the rolling and pitching. Substituting the estimates $\hat{\theta}(t)$ and $\hat{p}(t)$ obtained above into Equation 10.47 and subtracting the effect of the gravitational acceleration, one can derive a linear observation equation for $\alpha(t)$:

$$\begin{aligned} y_k &= \left[z_3(t) - g\cos\hat{\theta}(t)\cos\hat{p}(t) \right]_{t=k\Delta T} \\ &= H_k \mathbf{x}_k + v_k \end{aligned} \tag{10.58}$$

where $H_k = [0,0,\cos\hat{\theta}(t)\cos\hat{p}(t),0]\big|_{t=k\Delta T}$

$$v_k = v_3(k\Delta T)$$

Thus, the on-line measurement of the heaving is also realized by executing the same procedure as described before. The location of the rolling and pitching axes were assumed to be known; however, even when they are unknown, the attitude measurement system described above is effective, if we introduce the candidates on the location of the axes adding to the angular frequencies.

Attitude Measurement for Crane Lifters

Dynamics of Attitude Signals

An illustrative diagram of a crane lifter system is shown in Figure 10.11. One of the easiest ways to measure the attitude of the lifter is to set up a high-resolution camera on the bottom of the trolley and to track a mark on the top of the lifter. However, it increases the cost and also the difficulty in maintenance. Furthermore, sometimes the scheme does not work because of shadows and light reflection. As previously mentioned, for gyros not offering sufficiently accurate measurement, a high-sensitivity servo-type accelerometer is used to extract the attitude signals. When setting up the sensor on the lifter, however, there is a secondary swing signal adding to the primary one, due to the free suspension of the lifter and the structure of the lifter. Despite its small amplitude, the secondary one has a higher frequency and for this reason has a large magnitude on the sensor output. The important signal for practical applications, such as the attitude control of the lifter, is the primary one, which has a larger amplitude with a lower angular frequency of $\omega = \sqrt{g/\ell}$ (g: the gravitational acceleration; ℓ: the wire length from the primary supporting point to the center of gravity of the pulley). If we try to attenuate the secondary swing signal by passing the output through a low-pass filter, the phase lag is also introduced into the primary swing signal and the signal can no longer be used for the accurate attitude control of the lifter.

For the above reasons, we introduce an autonomous measurement system that measures both the primary and the secondary swings by modeling the lifter system with a double pendulum and applying a Kalman filter to it [14]. The dynamics of the trolley-lifter system is derived using Lagrange's equations of motion [8, 9].

$$\frac{d}{dt}\left(\frac{\partial T}{\partial \dot{x}}\right) - \frac{\partial T}{\partial x} + \frac{\partial V}{\partial x} = u - z\ddot{x} \tag{10.59}$$

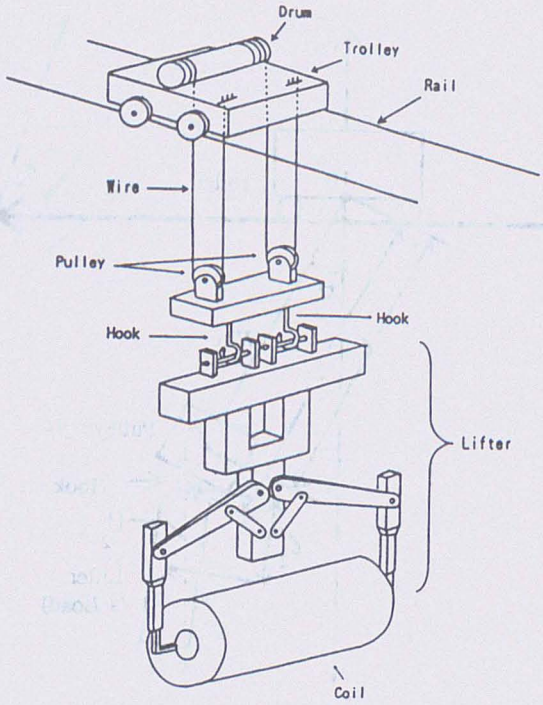

FIGURE 10.11 A crane lifter system.

$$\frac{d}{dt}\left(\frac{\partial T}{\partial \dot{\theta}_i}\right)-\frac{\partial T}{\partial \theta_i}+\frac{\partial V}{\partial \theta_i}=0 \quad (i=1,2) \tag{10.60}$$

where T and V represent, respectively, the kinetic and the potential energies of the trolley-lifter system, and θ_1, θ_2 denote, respectively, the angles that the primary and the secondary pendulums take against the vertical line. The other variables x, u, and a represent, respectively, the location of the trolley, the driving force, and the coefficient of friction between the trolley and the rail. Considering that θ_i, $\dot{\theta}_i$ ($1 \le i \le 2$) are small, the dynamic equation of the trolley-lifter system can be expressed as [14]:

$$\dot{\mathbf{x}}(t)=A\mathbf{x}(t)+\mathbf{b}u(t) \tag{10.61}$$

where $\mathbf{x}(t)$ is the state vector $\mathbf{x}(t) = x, \dot{x}, \theta_1, \dot{\theta}_1, \theta_2, \dot{\theta}_2)^T$. Taking into account the approximation errors in deriving Equation 10.61, air resistance, friction in the wires, and microscopic swings at the other connection points, it is reasonable to introduce white Gaussian noises $w(t)$ ($1 \le i \le 3$) with zero mean and appropriate variances to the dynamic Equation 10.61 as in Equation 10.49 as follows [14]:

$$\dot{\mathbf{x}}(t)=A\mathbf{x}(t)+\mathbf{b}u(t)+\Gamma\mathbf{w}(t) \tag{10.62}$$

where

$$\Gamma=\begin{bmatrix}0 & 1 & 0 & 0 & 0 & 0\\ 0 & 0 & 0 & 1 & 0 & 0\\ 0 & 0 & 0 & 0 & 0 & 1\end{bmatrix}^T, \qquad \omega(t)=\left[\omega_1(t),\ \omega_2(t),\ \omega_3(t)\right]^T \tag{10.62a}$$

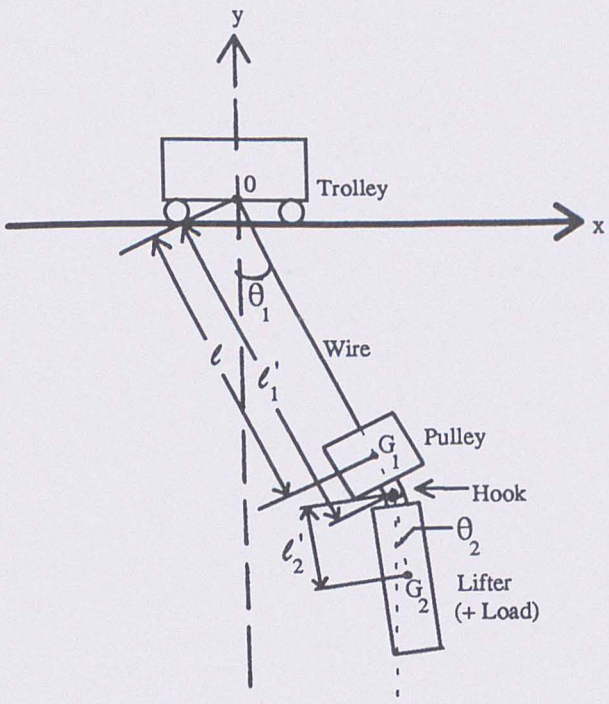

FIGURE 10.12 Dynamics of a trolley lifter system.

Sensor Outputs and On-Line Attitude Measurement

When a servo-type accelerometer is set up on the lifter (in the direction of the swing) at the place of the distance ℓ_2' from the secondary supporting point, the output of the sensor becomes [14]:

$$y(t) \cong -\ddot{x} - \ell_1'\ddot{\theta}_1 - \ell_2'\ddot{\theta}_2 - g\theta_2 \tag{10.63}$$

where ℓ_1' is the distance between the primary and the secondary supporting points (see Figure 10.12). Substitution of Equation 10.61 into Equation 10.63 yields an output expressed in terms of the state vector $\mathbf{x}(t)$, as in Equation 10.52. Using a rotary-encoder to measure the location and the velocity of the trolley, and then combining these three sensor outputs with the dynamic Equation 10.62 and applying a Kalman filter enables the state vector to be estimated on-line. Using this approach, both angular displacement and velocity of the deflections θ_1, θ_2 of the two pendulums can be measured exactly.

Aircraft Attitude Determination

The determination of aircraft attitude requires the measurement of angles about three independent body axes. These angles are the roll, pitch, and yaw angles. There are two primary means employed today for measuring these angles; the first method uses VGs to measure the roll and pitch angles, and a DG to measure the yaw angle. The second method, more commonly used today, employs an IMU for full three-axis attitude determination coupled with a baro-altimeter to correct for vertical drift errors in the IMU. Both methods are described below.

Vertical and Directional Gyro Analysis

A VG is a two degree-of-freedom gyro with its spin axis mounted nominally vertical. It employs two specific force sensors mounted nominally horizontal on the inner gimbal. The two angles measured by the VG — roll and pitch — require nearly identical analyses [1]. Consider the situation shown in

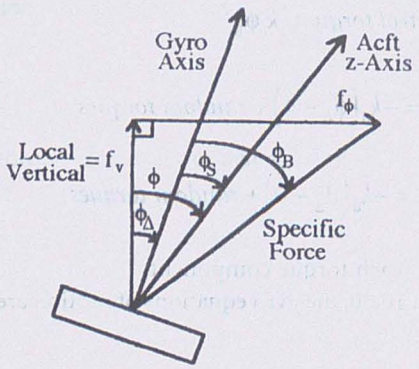

FIGURE 10.13 Vertical gyro analysis.

Figure 10.13, depicting an aircraft with a roll angle of ϕ with respect to the local vertical. The sensed roll angle ϕ_s is given by the difference in the actual roll angle and the gyro roll drift error ϕ_Δ:

$$\phi_s = \phi - \phi_\Delta \tag{10.64}$$

In order to compensate for this drift error, gyros employ a specific force sensor such as an electrolytic bubble device, which senses drift error. This correction device senses the angular difference between the specific force vector **f** acting on the aircraft roll axis and the gyro axis, as shown in Figure 10.13. Thus,

$$\phi_B = \tan^{-1}\left[\left(f_\phi / f_v\right) - \phi_\Delta\right] \cong \left(f_\phi / f_v\right) - \phi_\Delta \tag{10.65}$$

where f_ϕ is the side horizontal component of **f** and f_v = force of gravity is the vertical component. A similar analysis for the pitch angle θ yields:

$$\theta_s = \theta - \theta_\Delta \tag{10.66}$$

$$\theta_B = \tan^{-1}\left[f_\theta / f_v - \theta_\Delta\right] \cong f_\theta / f_v - \theta_\Delta \tag{10.67}$$

where f_θ is the back horizontal component of **f**. Next, define the gyro angular momentum vector by:

$$\mathbf{H}_{VG} = \left[J_x \dot{\phi}_\Delta,\ J_y \dot{\theta}_\Delta,\ -h\right] \tag{10.68}$$

where J_x and J_y are the sensor moments of inertia and h is the gyro spin angular momentum. In addition, define the inner gimbal axes angular velocity vector as:

$$\omega_{VG} = \left[\dot{\phi}_\Delta,\ \dot{\theta}_\Delta,\ 0\right] \tag{10.69}$$

Finally, define the gimbal torque vector by:

$$\mathbf{Q}_{VG} = \left[Q_{cx} + Q_{dx},\ Q_{cy} + Q_{dy},\ 0\right] \tag{10.70}$$

where

$$Q_{cx} = \textit{gimbal roll control torque} = -k_c \theta_B \tag{10.71a}$$

$$Q_{cy} = \textit{gimbal pitch control torque} = k_c \phi_B \tag{10.71b}$$

$$Q_{dx} = \textit{gimbal roll disturbance torque} = -k_d\left(\dot{\phi}_\Delta - \dot{\phi}\right) + \textit{random torques} \tag{10.71c}$$

$$Q_{dy} = \textit{gimbal pitch disturbance torque} = -k_d\left(\dot{\theta}_\Delta - \dot{\theta}\right) + \textit{random torques} \tag{10.71d}$$

and the k_c and k_d are constant scaling factors related to each torque component.

Using the vectors defined in Equations 10.68 through 10.70, the gyro equations of motion are given by:

$$\frac{\partial}{\partial t}\left(\mathbf{H}_{VG}\right) + \left(\omega_{VG} \times \mathbf{H}_{VG}\right) = \mathbf{Q}_{VG} \tag{10.72}$$

Taking the Laplace transform of the expansion of Equation 10.72, with the assumption that $J_x \cong J_y = J$, yields the following gyro equations of motion in the Laplace domain:

$$\begin{bmatrix} J_x s^2 + k_d s & -\left(hs + k_c\right) \\ hs + k_c & J_y s^2 + k_d s \end{bmatrix} \begin{bmatrix} \phi_\Delta(s) \\ \theta_\Delta(s) \end{bmatrix} \cong \begin{bmatrix} -k_c\theta_B + k_d s\phi(s) + \textit{random torques} \\ \left(k_c/g\right) f_\phi(s) + k_d s\theta(s) + \textit{random torques} \end{bmatrix} \tag{10.73}$$

For normal gyro operation, $J_x \cong J_y \cong 0$ and $k_d/h \ll 1$; so these factors may be ignored in Equation 10.73. Thus, solving for the desired roll and pitch angles under these assumptions gives [1]:

$$\phi_s = \begin{cases} \phi & \omega \gg k_c/h \\ \phi - f_\phi/g & \omega \ll k_c/h \end{cases} \tag{10.74}$$

$$\theta_s = \begin{cases} \theta & \omega \gg k_c/h \\ \theta - f_\theta/g & \omega \ll k_c/h \end{cases} \tag{10.75}$$

A DG is a two degree-of-freedom gyro with its spin axis mounted nominally horizontal and pointing in the direction of magnetic north. It employs a single specific force sensor mounted on the inner gimbal [1]. The DG measures the third required aircraft angle, yaw, generally denoted by ψ. The sensed yaw angle ψ_s is given by the difference in the actual yaw angle ψ (angle between the aircraft z-axis and true north) and the gyro heading angle drift error ψ_Δ (angle between the gyro axis and true north):

$$\psi_s = \psi - \psi_\Delta \tag{10.76}$$

Define the gyro angular momentum vector by:

$$\mathbf{H}_{DG} = \left[J_y\dot{\theta}_\Delta,\ J_z\dot{\psi}_\Delta,\ -h\right] \tag{10.77}$$

and the inner gimbal axes angular velocity vector as:

$$\omega_{DG} = \left[\dot{\theta}_\Delta,\ \dot{\psi}_\Delta,\ 0\right] \tag{10.78}$$

and the gimbal torque vector as

$$Q_{DG} = \left[Q_{cy} + Q_{dy}, Q_{cz} + Q_{dz}, 0 \right] \tag{10.79}$$

Here, the torque vector components are given by:

$$Q_{cy} = k_c \left(M_\Delta - \psi_\Delta \right) \tag{10.80a}$$

$$Q_{cz} = -k_c \theta_B \tag{10.80b}$$

$$Q_{dy} = -k_d \left(\dot{\theta}_\Delta - \dot{\theta} \right) + \textit{random torques} \tag{10.80c}$$

$$Q_{dz} = -k_d \left(\dot{\psi}_\Delta - \dot{\psi} \right) + \textit{random torques} \tag{10.80d}$$

where M_Δ = magnetic compass heading error (from true north). Therefore, the DG equations of motion are given in Laplace domain as:

$$\begin{bmatrix} J_y s^2 + k_d s & -\left(hs + k_c \right) \\ hs + k_c & J_z s^2 + k_d s \end{bmatrix} \begin{bmatrix} \theta_\Delta(s) \\ \psi_\Delta(s) \end{bmatrix} \cong \begin{bmatrix} k_c M_\Delta(s) + k_d s\theta(s) + \textit{random torques} \\ -k_c \theta_B + k_d s\psi(s) + \textit{random torques} \end{bmatrix} \tag{10.81}$$

The desired yaw angle measurement for the DG is thus given as [1]:

$$\psi_s = \begin{cases} \psi & \omega \gg k_c / h \\ \psi - M_\Delta & \omega \ll k_c / h \end{cases} \tag{10.82}$$

As indicated in Table 10.2, the accuracies of both VGs and DGs are approximately 1°. An improvement of over 2 orders of magnitude can be obtained through the use of inertial measurement units, which are described next.

Inertial Measurement Units (IMUs)

Inertial measurement units consist of gyroscopes and accelerometers that together provide full three-axis attitude measurements. Most are mounted on stable gimbaled platforms that remain locally horizontal via torquing devices. An IMU aboard an aircraft cannot measure exactly the local vertical due to the fact that the specific force acting on the aircraft has a horizontal component due to vehicle motion. In addition, since the vehicle is moving with respect to the inertial reference frame, the Earth's magnetic pole cannot be determined precisely [1].

These problems (errors) are minimized by aligning the IMU to be exactly horizontal and north pointing while the aircraft is stationary. Once platform motion begins, the IMU may be constantly realigned by sensing changes in the direction of vertical and north, and then applying appropriate torques to the platform to keep it properly aligned. This realignment is accomplished by integrating the two orthogonal accelerometer outputs to determine the components of horizontal velocity. This data, combined with the Earth's rotation rate, yields the desired rates of change in local vertical and true north at the vehicle's current latitude and longitude. Performing a second integration of the sensor outputs yields an estimate of relative position.

Analysis in Bryson et al. [1], has shown that the pitch angle (variation in platform horizontal position) is given by the IMU sensor output as:

$$\theta(t) = \frac{-\varepsilon}{\omega_s} \sin(\omega_s t) - \frac{b}{g} \tag{10.83}$$

where ε = gyro drift rate error, b = specific force sensor error, and $\omega_s \equiv$ Schuler frequency = $\sqrt{g/R}$, [g = force of gravity, R = Earth's radius]. Thus, the platform root-mean-square pitch angle becomes:

$$\theta_{rms} = \left[\frac{1}{2}\left(\frac{\varepsilon}{\omega_s}\right)^2 + \left(\frac{b}{g}\right)^2\right]^{\frac{1}{2}} \tag{10.84}$$

Using typical values for ε ($\cong 0.015° \text{ h}^{-1}$), ω_s ($\cong 0.71° \text{ h}^{-1}$), and b ($\cong 0.01$) yields an rms pitch angle error of $\theta_{rms} = 0.01°$. Thus, it is apparent that under normal operating conditions the IMU provides a two orders-of-magnitude improvement in sensor accuracy when compared to the VG and DG.

Spacecraft Attitude Determination

Most spacecraft attitude determination techniques rely upon finding the orientation of a single axis in space (e.g., the spacecraft z-axis) plus the spacecraft rotation about this axis. This provides a full three-axis attitude solution. In order to achieve this, reference sources that are external to the spacecraft must be used. Specifically, full three-axis spacecraft attitude determination requires at least two external vector measurements. Commonly used reference sources for these external vector measurements include the sun, Earth, moon, stars, planets, and the Earth's magnetic field. In addition, IMUs are also used to provide the necessary attitude measurements.

Attitude Determination Methodology

The first step in attitude determination is to determine the angles between the spacecraft's primary axis and the two (or more) attitude reference sources. For example, suppose a particular spacecraft is using the sun and the Earth for attitude reference. The two angles in this case are referred to as the sun angle β_S and the nadir angle Γ_N. Since the orientation of even a single spacecraft axis is unknown at this point, these angles establish two *cones* along which the attitude vector **A** must lie. Since the attitude vector must lie on both cones, it must lie along the intersection between the two cones [4] (See Figure 10.14). The two vectors, notably $\mathbf{A}_1$ and $\mathbf{A}_2$, resulting from the intersection of these two cones may be determined by the following method derived by Grubin [15]. Let **S** represent the sun vector, **E** the spacecraft nadir vector, and **A** the desired attitude vector, each defined in Cartesian space as follows:

$$\mathbf{S} = (S_x, S_y, S_z) \tag{10.85}$$

$$\mathbf{E} = (E_x, E_y, E_z) \tag{10.86}$$

$$\mathbf{A} = (A_x, A_y, A_z) \tag{10.87}$$

Let the vectors **S**, **E**, and **N** define a set of base unit vectors with:

$$\mathbf{N} = \frac{\mathbf{S} \times \mathbf{E}}{|\mathbf{S} \times \mathbf{E}|} = (N_x, N_y, N_z) \tag{10.88}$$

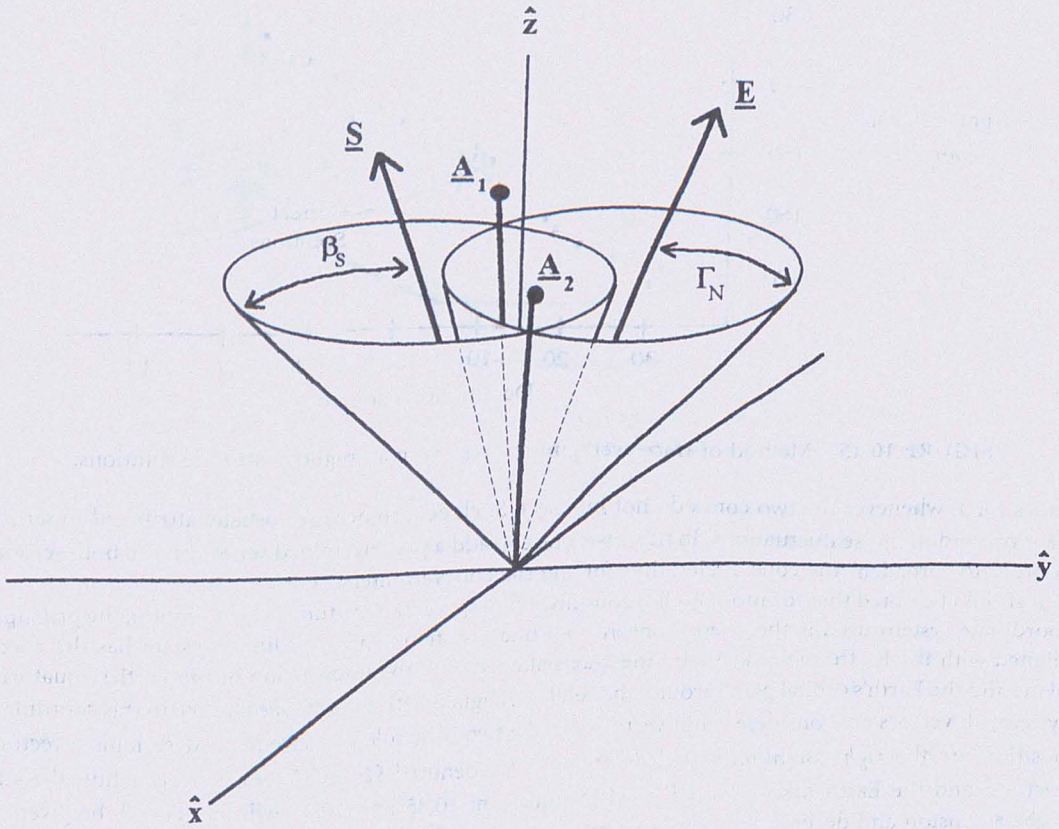

FIGURE 10.14 Relationship between reference vectors and single-axis attitude cones.

If we introduce a proper set of scaling factors as follows:

$$I_x = \frac{\left[\cos\beta_S - (\mathbf{S}\cdot\mathbf{E})\cos\Gamma_N\right]}{1-(\mathbf{S}\cdot\mathbf{E})^2} \tag{10.89a}$$

$$I_y = \frac{\left[\cos\Gamma_N - (\mathbf{S}\cdot\mathbf{E})\cos\beta_S\right]}{1-(\mathbf{S}\cdot\mathbf{E})^2} \tag{10.89b}$$

$$I_z = \sqrt{1 - I_x\cos\beta_S - I_y\cos\Gamma_N} \tag{10.89c}$$

then the two possible attitude vectors $\mathbf{A}_1$ and $\mathbf{A}_2$ are found to be:

$$\mathbf{A}_{1,2} = \left[\left(I_x S_x + I_y E_y \pm I_z N_x\right), \left(I_x S_y + I_y E_y \pm I_z N_y\right), \left(I_x S_z + I_y E_z \pm I_z N_z\right)\right] \tag{10.90}$$

In Equations 10.88 through 10.90, $\mathbf{S}\times\mathbf{E}$ represents the Cartesian vector product, and $\mathbf{S}\cdot\mathbf{E}$ represents the Cartesian scalar product. The radicand in Equation 10.89c may be negative, thus producing imaginary

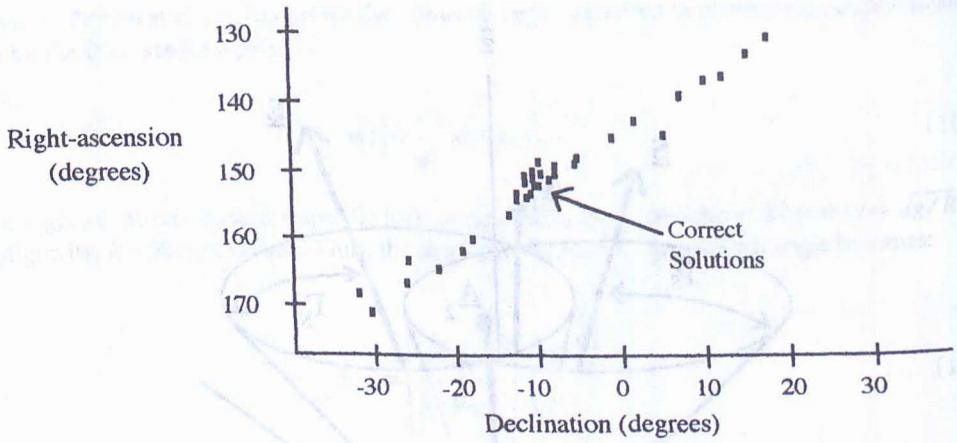

FIGURE 10.15 Method of trace averaging for resolving ambiguous attitude solutions.

values for I_z whenever the two cones do not intersect. Such occurrences are usually attributed to sensor error or random noise fluctuations. In this case, one can add a predetermined sensor bias to both sensors in order to "broaden" the cone angles, thus forcing the cones to intersect.

It should be noted that for most applications involving spacecraft attitude determination, the principle coordinate system used is the *celestial sphere* coordinate system. This coordinate system has the *z*-axis aligned with the Earth's polar axis, and the *x*-axis aligned with the intersection of the Earth's equatorial plane and the Earth's orbital plane around the sun (i.e., aligned with the *vernal equinox*). In this coordinate system, all vectors are considered unit vectors and the two principle measurements describing a vector's position are the *right-ascension* and *declination angles*, denoted Ω and Δ, respectively. Thus, the sun vector **S** and the Earth nadir vector **E** used in Equations 10.85 and 10.86 will, in general, be given as right-ascension and declination angles that can be converted to Cartesian coordinates via the following set of transformations:

$$x = \cos(\Omega)\cos(\Delta); \quad y = \sin(\Omega)\cos(\Delta); \quad z = \sin(\Delta) \tag{10.91a}$$

$$\Omega = \tan^{-1}(y/x); \quad \Delta = \sin^{-1}(z) \tag{10.91b}$$

The final step in measuring three-axis attitude is to determine which attitude solution is correct, A_1 or A_2, and then measure the rotation about this axis. The two ambiguous attitude solutions may be resolved by comparison with a priori attitude information, if available, or through the use of *trace averaging* [4]. Trace averaging is a method of plotting each attitude solution on a right-ascension versus declination plot and choosing the area of greatest concentration as the correct solution, as demonstrated in Figure 10.15. Since the attitude is assumed to change more slowly than the attitude sensor's sample rate, over short time intervals the data for the correct solution usually form a "cluster" near the correct attitude; the data for the incorrect solution are usually much more scattered.

Once the correct attitude vector has been obtained, the orientation of the remaining two orthogonal axes may be found by measuring the rotation, or phase angle, of the spacecraft about the preferred axis. Any sensor measurement that provides this phase angle may be used. An example of this technique is provided by the panoramic annular lens attitude determination system (PALADS), described in the next section. This imaging system uses a unique "three-dimensional" lens that provides simultaneous detection of two (or more) reference sources [16]. This information, combined with the orientation of the single axis, uniquely determines three-axis attitude.

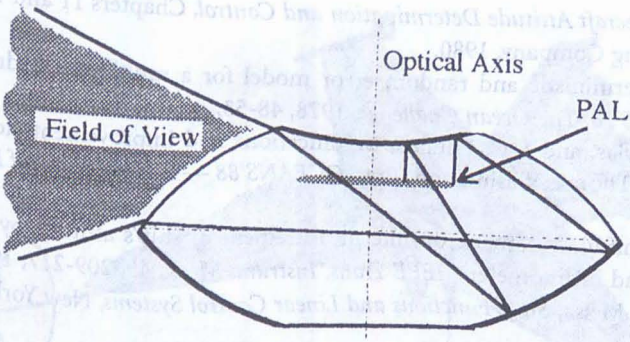

FIGURE 10.16 Panoramic annular lens ray diagram.

The three angles derived above, which are commonly referred to as *Euler angles*, define the orientation of the three spacecraft axes with respect to the chosen reference frame. A more formal treatment of the attitude solution usually requires specifying the components of the 3×3 attitude matrix **A**. Each component of the attitude matrix defines the angular relationship between a given spacecraft axis and a reference frame axis. Various methods exist for computing the attitude matrix **A** (see [4]); the preferred method depends on the particular application at hand.

PALADS

The primary component of PALADS is the panoramic annular lens (PAL), a single-element lens made from a high index of refraction glass with certain portions of the lens coated with a mirrored surface. Hence, it relies on both refraction and reflection in forming an image (Figure 10.16). The lens is unique in that it images a three-dimensional object field onto a two-dimensional image plane, whereas a "normal" lens is capable of only imaging two-dimensional object space onto an image plane. The combination of high index of refraction glass and mirrored surfaces provides the PAL with a field of view extending from approximately 65° to 110° from the optical axis. This 45° field of view covers the entire 360° surrounding the optical axis [17]. Any ray originating from outside the 45° field of view will not form a part of the image. The PAL may be attached to any high-quality imaging system using an appropriate *transfer lens.* As currently configured, the PALADS imaging system utilizes a Sony XC-73 charged-couple device (CCD), a black and white video camera coupled to the PAL via a Nikon *f*/1.4 transfer lens.

The hemispherical view provided by PALADS allows for single-sensor detection of multiple attitude reference sources, such as the Earth and the sun or moon. The position of each reference source in the image plane translates into a unique azimuth elevation angle between the PAL's optical axis and the reference source. Since the PAL has a 360° field of view surrounding the optical axis, it may detect several reference sources simultaneously. The data points associated with each source are extracted from the image plane using digital image processing techniques. Thus, it is easy to see how a single image from PALADS (containing two or more reference sources) provides the necessary angle data to determine three-axis spacecraft attitude.

References

1. A. E. Bryson, *Control of Spacecraft and Aircraft*, Chapter 10, Princeton, NJ: Princeton University Press, 1994.
2. W. J. Larson and J. R. Wertz (eds.), *Space Mission Analysis and Design*, Chapter 11, Torrance, CA: Microcosm Inc. and Dordrecht, The Netherlands: Kluwer Academic Publishers, 1992.
3. NASA Technical Memorandum NASA TM X-64757, *Terrestrial Environment (Climatic) Criteria Guidelines for Use in Aerospace Vehicle Development (1973 Revision)*, Marshall Space Flight Center, AL, 1973.

4. J. R. Wertz (ed.), *Spacecraft Attitude Determination and Control*, Chapters 11 and 12, The Netherlands: Reidel Publishing Company, 1980.
5. R. D. Angelari, A deterministic and random error model for a multibeam hydrographic sonar system, *Proc. OCEANS'78. The Ocean Challenge*, 1978, 48-53.
6. C. de Moustier, T. Hylas, and J. C. Phillips, Modifications and improvements to the Sea Beam system on board R/V Thomas Washington, *Proc. OCEANS'88 — A Partnership of Marine Interests*, 1988, 372-378.
7. S. Tanaka and S. Nishifuji, Automatic on-line measurement of ship's attitude by use of a servo-type accelerometer and inclinometers, *IEEE Trans. Instrum. Meas.*, 45, 209-217, 1996.
8. D. G. Shultz and J. L. Melsa, *State Functions and Linear Control Systems*, New York: McGraw-Hill, 1967.
9. Y. Takahashi, M. J. Rabins, and D. M. Auslander, *Control and Dynamic Systems*, Reading, MA: Addison-Wesley, 1971.
10. S. Tanaka and S. Nishifuji, On-line sensing system of dynamic ship's attitude by use of servo-type accelerometers, *IEEE J. Oceanic Eng.*, 20, 339-346, 1995.
11. S. Tanaka, On automatic attitude measurement system for ships using servo-type accelerometers (in Japanese), *Trans. SICE*, 27, 861-869, 1991.
12. D. E. Cartwright and M. S. Longuet-Higgins, The statistical distribution of the maxima of a random function, *Proc. Roy. Soc. London*, Ser. A, 237, 212-232, 1956.
13. R. E. Kalman, A new approach to linear filtering and prediction problems, *Trans. ASME, J. Basic Eng.*, 82, 35-45, 1960.
14. S. Tanaka, S. Kouno, and H. Hayashi, Automatic measurement and control of attitude for crane lifters (in Japanese), *Trans. SICE*, 32(1), 97-105, 1996.
15. C. Grubin, Simple algorithm for intersecting two conical surfaces, *J. Spacecraft Rockets*, 14(4), 251-252, 1977.
16. M. A. Stedham and P. P. Banerjee, The panoramic annular lens attitude determination system, *SPIE Proceedings, Space Guidance, Control, and Tracking II*, Orlando, FL, 17-18 April, 1995.
17. J. A. Gilbert, D. R. Matthys, and P. Greguss, Optical measurements through panoramic imaging systems, *Proc. Int. Conf. Hologram Interferometry and Speckle Metrology*, Baltimore, MD, November 4-7, 1990.